Journal of Solution Chemistry
https://doi.org/10.1007/s10953-025-01436-5

Computational Exploitation of Verbenone Encapsulation by β–Cyclodextrin: Revealing Structure, Energies, and Non-covalent Interactions.

Souha Fatma Zohra Soukehal[1] · Djamel Bouchouk[1] · Tahar Abbaz[1] · Didier Villemin[2]

Received: 22 July 2024 / Accepted: 26 January 2025

Abstract
Despite having significant pharmaceutical potential, many compounds are avoided by researchers due to their low solubility and high volatility. These characteristics make them difficult to manipulate and incorporate into drug formulations. Cyclodextrins solve this problem by increasing the solubility of bioactive molecules, making them easier to handle and significantly improving bioavailability. These macromolecules have a wide range of applications, including pharmaceuticals, agriculture, cosmetics, and the environment. This paper presents a computational study of an inclusion complex between verbenone and β–cyclodextrin (β–CD) with a 1 : 1 stoichiometry. The objective is to improve understanding of anomalies that were not identified during experiments and explain why verbenone forms a good complex with β–cyclodextrin. This complex aims to increase verbenone solubility while decreasing volatility for maximum activity. The PM3 method was used to optimize the verbenone*β–cyclodextrin complex as a first excess. The guest was oriented once toward the wide side of the β–CD (orientation A) and another toward the narrow side (orientation B), with inclusion simulation using hyperchem 8.0 software. After calculating the complexation energies and determining the optimal complexes, these complexes were re-optimized using density function methods: B3LYP, MN15, and MN15L with a base set 6-31 G(d,p) in gas and aqueous phases. Theoretical calculations were performed with Gaussian16 software, and visualization was carried out using Gaussview 6. According to the optimal 3D structures, the verbenone was fully encapsulated in the β–CD cavity. The complexation energies, HOMO-LUMO orbitals, and reactivity parameters were calculated. Their analysis confirms that the complex at orientation A is more stable and electrophilic than that at orientation B, and the charge is transferred from the host to the guest. Natural binding orbitals (NBO) were also analyzed. The QTAIM, RDG-NCI, and IGM analyses were interpreted to consider the non-covalent interactions that maintain stability between β–CD and verbenone. Data analysis and visualization were performed using Multiwfn and VMD. The chemical shifts of verbenone protons in the free and complex states were calculated and compared to experimental data. The findings show the formation of a complex between verbenone and β–CD, which is stabilized by van der Waals and hydrogen interactions.

Djamel Bouchouk, Tahar Abbaz, and Didier Villemin have contributed equally to this work.

Extended author information available on the last page of the article

Keywords Verbenone · β–cyclodextrin · Inclusion complex · DFT · NBO · QTAIM

1 Introduction

Cyclodextrins are cyclic oligosaccharides. The most popular cyclodextrins are $\alpha-$, $\beta-$, and $\gamma-$cyclodextrin, which differ from each other by the number of glucose units contained in their molecules ($\alpha-$six, $\beta-$seven, $\gamma-$eight). An $\alpha-(1 \rightarrow 4)$ bond [1] connects these units, resulting in a tonic conical cycle with a hydrophilic external surface and a hydrophobic internal cavity. Several references demonstrate that CDs' have a specific structure that allows them to form water-soluble inclusion complexes with various hydrophobic compounds, whether solid, liquid, or gaseous [2–5]. Cyclodextrins are commonly used as hosts for pharmaceutical, agrifood, or even cosmetic molecules to enhance their water solubility, chemical and physical stability, and bioavailability [6].

The present study uses $\beta-$cyclodextrin as the host due to its non-toxicity, reactivity, biocompatibility, and low cost [7]. Verbenone, a monoterpene, was chosen as a guest. This molecule can be derived from the essential oils of certain plants, primarily rosemary, or it can be produced by certain germs and bacteria [3]. It can also be synthesized from pinene as was performed in Ref. [8]. The authors in Ref. [9] found that the enantiomers of verbenone have antifungal, antibacterial, anticandidal, and antibiofilm properties. It also has anti-inflammatory potential on a model of a cutaneous cellular system with no toxic effect at the concentration tested. This study also reveals that despite the high level of chirality in monoterpenes, which can influence their biological properties, the two verbenone enantiomers exhibit similar biological activity. Thus, verbenone, a volatile organic compound (VOC) with hydrophobic [10] properties, can be encapsulated in the $\beta-$CD cavity to reduce its volatility and increase its solubility in water.

Halahlah et al. [3] introduced the verbenone $\beta-$cyclodextrin complex, which was used to encapsulate Roman essential oil in β-cyclodextrin. Verbenone is one of the most volatile constituents of this oil, exhibiting preferential incorporation into the $\beta-$cyclodextrin cavity. This was attributed to the presence of a carbonyl group, which makes it a good hydrogen bond acceptor and facilitates interaction with the cyclodextrin cavity. Subsequently, Nakhle et al. [11] synthesized the complex and studied its ability to encapsulate $\beta-$CD with verbenone in water and deep eutectic solvents (DES:water). The findings confirm the correct formation of the verbenone*$\beta-$CD complex, whether in an aqueous medium or solvents (DESs), as determined by the following methods: SH-GC, NMR, and ITC. All these synthesis studies confirm verbenone's suitability as a guest in $\beta-$CD. Despite the wealth of information gleaned from data analysis, several issues remain unclear. For example, it is impossible to definitively determine the geometry of this complex, its orientation within the cavity, or the specific intermolecular interactions that contribute to its stability.

This paper presents a theoretical study of the verbenone*$\beta-$CD complex to explain the anomalies in the inclusion mechanism and determine the nature of the interaction between $\beta-$CD and verbenone. To this end, the 1 : 1 encapsulation of verbenone inside the $\beta-$CD cavity was examined using quantum mechanics methods such as the semi-empirical method PM3 and the functional theory of density (DFT). First, we decided to start the theoretical excesses with the semi-empirical method PM3 [12] to evaluate its performance in finding the optimal complex having the lowest energy at orientation A and B while waiting to compare it with other semi-empirical methods (PM6 [13] PM7 [14]) used in other works. Then, we optimized the optimal complexes in the gaseous and aqueous mediums with

the methods B3LYP [15], MN15 [16], and MN15L [17], using the 6-31 G(d,p) base set. Following that, a frontier orbital analysis was carried out to describe the charge flow and investigate the complexes' stability. To determine the nature of the interactions between the host and the guest, we examined the natural orbitals (NBO), the quantum theory atom in the molecule (QTAIM), the non-covalent interaction-reduced density gradient (NCI-RDG), and the independent gradient model (IGM).

2 Computational Details

The initial structures of verbenone and β−cyclodextrin were obtained from the PubChem database [18]. The Hyperchem 8.0 software [19] was used for complication and guest translation on the *Z* axis. Gaussian 16 [20] was used to perform theoretical calculations, while Gaussview 6 [21] was employed for visualization. The QTAIM, NCI-RDG, and IGM analyses were obtained using the Multiwfn software [22], visualized by VMD [23]; Gnuplot [24] was to obtain the colored graphs. Figure 1 shows the optimized structures and atom numbering of each host and guest [25]. To complete the complexing process, the glycosidic oxygen atoms of β−CD were placed in the *XY* plane, and their center was defined as the center of the entire system. Verbenone was placed on the *Z* axis, which was aligned with the atoms O167, C151, and C164 [26, 27].

The host's (β−CD) maintained its position, while the guest moved along the *Z* axis. It then crossed the cyclodextrin cavity, passing once from the wide side to the narrow side of the CD, called orientation A, and once from the narrow side to the wide side, called orientation B (Fig. 2). The guest molecule was initially positioned at 6 Å and moved through Z to -6 Å, or vice versa, with a step size of 1 Å [28]. To find the most stable conformer of the complex, in each position, a rotation around the Z axis of 360° was performed on the guest molecule with an interval of 3°. The PM3 semi-empirical method was used to optimize the Verb*β−CD complex at each position and angle. The lowest energy was determined

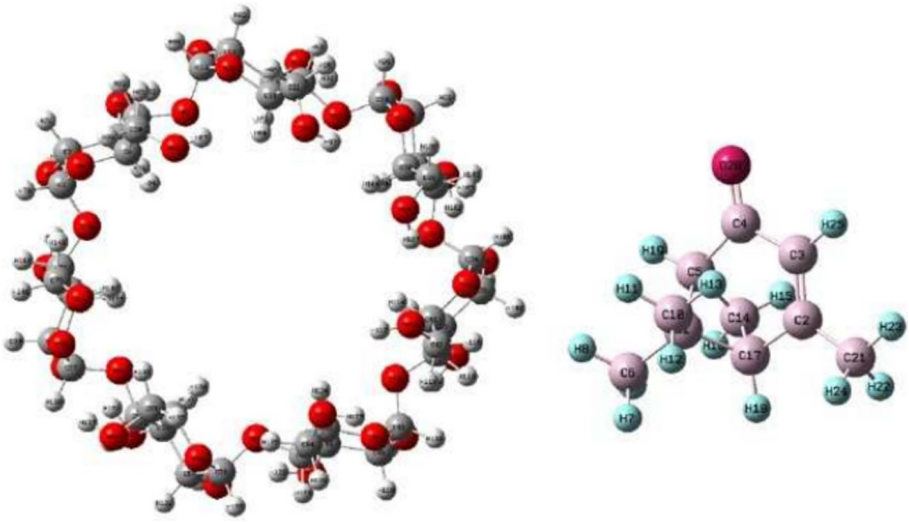

Fig. 1 The molecular structure of β−CD and Verbenone

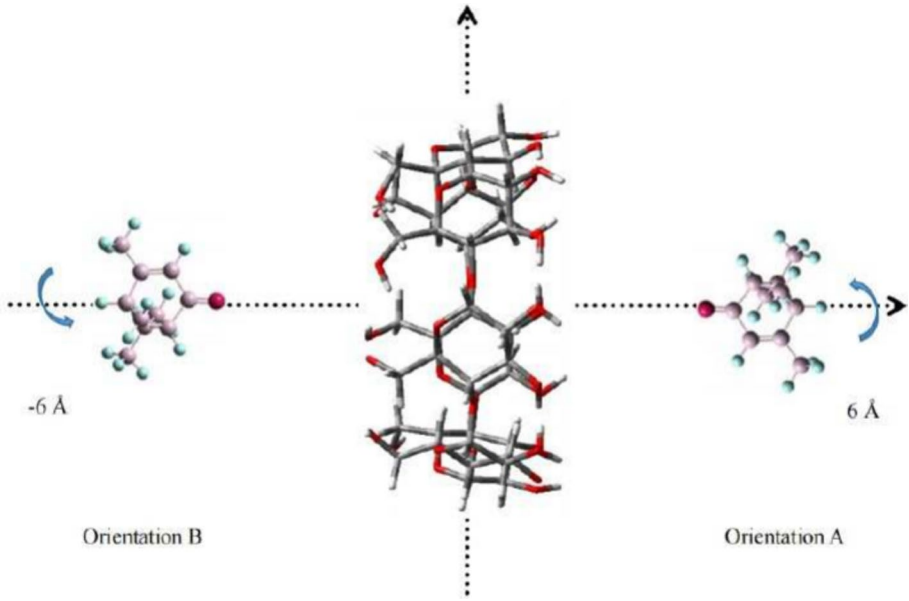

Fig. 2 A schematic representation of the inclusion process between Verbenone and β−CD in both orientations A and B

by interpreting two curves for orientations A and B. The position with the lowest energy for the two orientations is then re-optimized using the mentioned density functional theory (DFT) methods [26] B3LYP/6-31 G(d,p), MN15/6-31 G(d,p), and MN15L/6-31 G(d,p).

3 Results and Discussions

3.1 The Energy and Structural Analysis of Complexes

The complexation energy ($E_{\text{complexation}}$) of the inclusion complex Verb*β−cyclodextrin was calculated using Eq. 1 [29]:

$$E_{\text{complexation}} = E_{\text{Verb}*\beta-\text{CD}} - (E_{\beta-\text{CD}} + E_{\text{Verb}}), \tag{1}$$

where $E_{\text{Verb}*\beta-\text{CD}}$ is the energy of the complex optimized by the semi-empirical method PM3, and $E_{\beta-\text{CD}}$ and E_{Verb} are the energies of the verbenone and the β−cyclodextrin, respectively, before complexation which are also optimized by the same method. Figure 3 depicts the complexation energy at all positions of the complex in orientations A and B. These energies obtained are negative, indicating that the Verb*β−cyclodextrin complexes are energetically favorable.

The optimal position is the one with the lowest energy for the two orientations; this is where the complex is most stable. Table 1 lists the optimal position for orientations A and B: 0 Å for orientation A and 1 Å for orientation B, with a rotation angle of 0° for both. The interaction energy demonstrates that the Verb*β−cyclodextrin complex at orientation A is more stable by 3.464 kJ · mol^{-1} than the complex at orientation B.

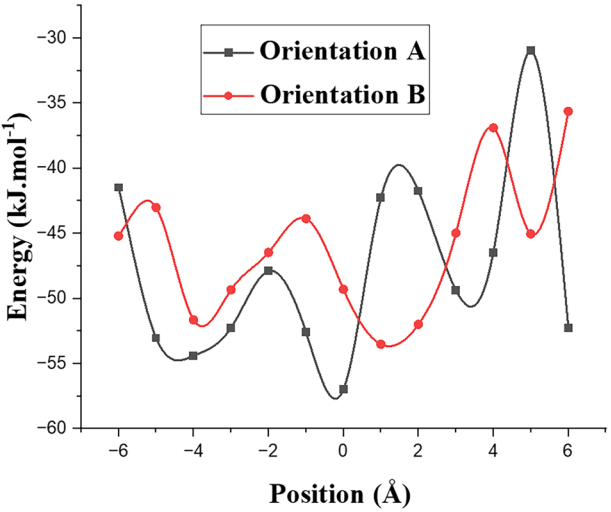

Fig. 3 The complexation energies of the Verb*β−CD in each position for orientation A and B

Table 1 The coordinates of the optimal conformation for the complex

PM3	Orientation A	Orientation B
Optimal position (Å)	0	1
Angle(°)	0	0
Energy (J·mol^{-1})	− 56.919	− 53.454

The optimal position obtained for orientations A and B was then re-optimized in the gas and aqueous phases using the methods B3LYP/6-31 G(d,p), MN15/6-31 G(d,p), and MN15L/6-31 G(d,p). In this step, a PCM (Polarizable Continuum Model) model was employed; this solvation model is implicit. The PCM solvation model considers the solvent as a continuous medium, accounting for its impact on fragment properties such as structure, energy, and reactivity as noted in Ref. [30]. According to Ref. [31], PCM is the most accurate model for predicting molecular structure. Water was chosen as a solvent based on the experimental study in Ref. [11]. The authors indicated that the Verb*β−cyclodextrin complex is more stable in water compared to a (DES:water) mixture. This phenomenon is explained by the hydrophobic effect, which is less pronounced in the (DES:water) mixture due to its lower polarity when compared to water. Table 2 displays the energy values for orientations A and B in both phases. All of the energies calculated for orientation A are lower than those calculated for orientation B, indicating that orientation A has better complexation than orientation B. The interaction energy ($E_{\text{Interaction}}$) can be calculated using Eq. 2 [29]:

$$E_{\text{Interaction}} = E_{\text{Verb}*\beta-\text{CD}} - (E^{sp}_{\beta-\text{CD}} + E^{sp}_{\text{Verb}}), \tag{2}$$

where $E_{\text{Verb}*\beta-\text{CD}}$ is the energy of the optimized complex, $E^{\text{sp}}_{\beta-\text{CD}}$ and $E^{\text{sp}}_{\text{Verb}}$ are the energies of the verbenone and the β−cyclodextrin, respectively, before complexation which are also optimized by the three methods.

Table 2 The different energies ($kJ \cdot mol^{-1}$) of the complex calculated by the B3LYP/6-31(d,p) method, MN15/6-31(d,p) and MN15L/6-31(d,p) in orientation A and B in the gas and aqueous phase

Energies	In gas phase			In aqueous phase		
	Orientation A	Orientation B	Difference	Orientation A	Orientation B	Difference
B3LYP/6–31(d,p)						
$\Delta E_{complexation}$	− 18.4263	− 2.9716		− 27.032	− 14.6279	
$\Delta E_{interaction}$	− 59.4860	− 92.8840		− 181.9261	− 19.3388	
$E_{DEF(\beta-CD)}$	39.9658	27.7063	12.2595	17.3595	4.3514	3.0499
$E_{DEF(Verb)}$	1.0935	0.5793	0.5142	1.2066	0.3591	0.8475
MN15/6–31(d,p)						
$\Delta E_{complexation}$	− 100.1628	− 91.6491		− 106.2615	− 96.7607	
$\Delta E_{interaction}$	− 155.7618	− 168.0974		− 150.0191	− 138.7756	
$E_{DEF(\beta-CD)}$	52.4565	73.3327	20.8762	39.4805	39.3652	1153
$E_{DEF(Verb)}$	3.1421	3.2157	0.0736	0.4448	2.6489	7959
MN15L/6–31(d,p)						
$\Delta E_{complexation}$	− 165.4089	137.8209		− 166.4505	− 140.3886	
$\Delta E_{interaction}$	− 232.1371	205.6978		− 199.5917	− 181.6443	
$E_{DEF(\beta-CD)}$	56.7790	63.0557	6.2767	25.1331	37.0912	11.9602
$E_{DEF(Verb)}$	9.9488	4.6636	5.2852	8.0076	4.1650	3.8426

The MN15L/6-31 G(d,p) method yielded lower energy values in the gas phase (232.137 $kJ \cdot mol^{-1}$ for orientation A, 205.698 $kJ \cdot mol^{-1}$ for orientation B) and the aqueous phase (199.592 $kJ \cdot mol^{-1}$ for orientation A, 181.644 $kJ \cdot mol^{-1}$ for orientation B). The inclusion energy was then calculated using the ML15/6-31 G(d,p) method, yielding −155.762 $kJ \cdot mol^{-1}$ for orientation A, −168.097 $kJ \cdot mol^{-1}$ for orientation B in the gas phase, and −150.191 $kJ \cdot mol^{-1}$ for orientation A and −138.776 $kJ \cdot mol^{-1}$ for orientation B in the aqueous phase. The B3LYP/6-31(d,p) method had the highest interaction energy, with values of 59.486 $kJ \cdot mol^{-1}$ for orientation A, −31.258 $kJ \cdot mol^{-1}$ for orientation B in the gas phase, and −181.926 $kJ \cdot mol^{-1}$ for orientation A and −19.339 $kJ \cdot mol^{-1}$ for orientation B in the aqueous phase. The energy of complexation can be calculated using Eq. 1. The complexation energy obtained by the MN15L/6-31 G(d,p) method was the lowest energy, with 165.409 $kJ \cdot mol^{-1}$ for orientation A and 137.821 $kJ \cdot mol^{-1}$ for orientation B in the gas phase and 166.451 $kJ \cdot mol^{-1}$ for orientation A and 136.209 $kJ \cdot mol^{-1}$ for orientation B in the aqueous phase, respectively. Whereas the MN15/6-31 G(d,p) method gave 100.163 $kJ \cdot mol^{-1}$ for orientation A and 91.5479 $kJ \cdot mol^{-1}$for orientation B in the gas phase, and 106.272 $kJ \cdot mol^{-1}$ for orientation A, and 96.7607 $kJ \cdot mol^{-1}$ for orientation B in the aqueous phase. The B3LYP/6-31(d,p) method, on the other hand, presented the highest energy values, with −18.426 $kJ \cdot mol^{-1}$ for orientation A, −2.9716 $kJ \cdot mol^{-1}$ for orientation B in the gas phase, and −27.0032 $kJ \cdot mol^{-1}$ for orientation A and −14.6279 $kJ \cdot mol^{-1}$ for orientation B in the aqueous phase. Therefore, based on the complexation and interaction energies obtained, the methods MN15/6-31 G(d,p) and MN15L/6-31 G(d,p) appear to be the most suitable.

The deformation energy of the host and guest was determined by the energy difference between the compound during complexation and when it is free, calculated by Eq. 3 [32]:

$$E^{\mathrm{DFT}}_{(\beta-\mathrm{CDorVerb})} = E^{\mathrm{OPT}}_{\mathrm{sp}(\beta-\mathrm{CDorVerb})} - E^{\mathrm{OPT}}_{(\beta-\mathrm{CDorVerb})} \quad (3)$$

where $E^{\mathrm{OPT}}_{\mathrm{sp}(\beta-\mathrm{CDorVerb})}$ is the single-point energy of the isolated β−cyclodextrin and verbenone from the complex and $E^{\mathrm{OPT}}_{(\beta-\mathrm{CD}or\mathrm{Verb})}$ is the energy of these compounds in the free start after optimization.

In the guest deformation energies for the B3LYP/6-31(d,p) and MN15L/6-31 G (d,p) methods, the energy required for complexation with the guest is greater in the A orientation than in the B for both phases. The energy difference between the A and B orientations of the Verb*β−cyclodextrin complex for the B3LYP/6-31(d,p) method was approximately 0.5141 kJ · mol^{-1} in the gas phase and 0.8476 kJ · mol^{-1} in the aqueous phase. For the MN15L/6-31(d,p) method, this difference is approximately 5.285 kJ · mol^{-1} in the gas phase and 3.8427 kJ · mol^{-1} in the aqueous phase. However, for the MN15/6-31(d,p) method, the energy required for complexation in orientation B is greater than that in orientation A, with a difference of 0.0736 kJ · mol^{-1} for the gas phase and 2.204 kJ · mol^{-1} in the water. The higher deformation energy of β−cyclodextrin compared to verbenone suggests that its flexibility is responsible for the complexation of the verb*β−cyclodextrin system proven in Ref. [25]. In methods MN15/6-31(d,p) and MN15L/6-31(d,p), orientation B requires more energy than orientation A, with a difference of 20.876 kJ · mol^{-1} in the gas phase and 0.1154 kJ · mol^{-1}in the aqueous phase for method MN15/6-31(d,p), and a difference of 6.2767 kJ · mol^{-1} in the gas phase and 11.9581 kJ · mol^{-1} in the aqueous phase for the MN15L/6-31(d,p) method. These findings indicate that complexation in orientation A is more favorable than that in orientation B, and that cyclodextrin deformations are necessary to form a stable inclusion complex [33]. Compared to other methods, the B3LYP/6-31(d,p) method requires more energy for orientation A than for orientation B, with a difference of 12.2595 kJ · mol^{-1} in the gas phase and 13.008 kJ · mol^{-1} in the aqueous phase. In light of the energy results, we decided to continue this work only with the two best methods, MN15/6-31(d,p) and MN15L/6-31(d,p). The DFT calculations did not explicitly include dispersion effects or BSSE because the new MN15 and MN15L functionals were utilized. These functionals have been shown to provide accurate results for a wide variety of molecular properties, including non-covalent interactions, ionization potentials, and electron affinities, while also reducing BSSE. The local nature of the calculations reduces computational costs, making it possible to investigate larger and more complex systems without requiring additional dispersion corrections confirmed in the articles [16, 17]. This provides a significant advantage in terms of computational efficiency. Figure 4 shows the structures of the optimal conformations of the Verb*β−cyclodextrin complex with the three methods B3LYP/6-31(d,p), MN15/6-31 G(d,p), and MN15L/6-31 G(d,p) in orientations A and B in the aqueous phase. It can be noted that the verbenone molecule is completely enveloped by β−cyclodextrin. This is due to the hydrophobic nature of the verbenone molecule, which contains a benzene ring, a non-polar molecule [25]. The cyclodextrin cavity exhibits hydrophobic characteristics, facilitating intermolecular interactions between the hydroxyl groups of CD and the hydrophobic groups of verbenone. This improves the stability of the Verb*β−cyclodextrin complex.

3.2 The Frontier Molecular Orbital Analysis

The density functional theory (DFT) was applied to analyze the frontier orbitals, enhance comprehension of the inclusion phenomenon, and determine the stability of the Verb *β−

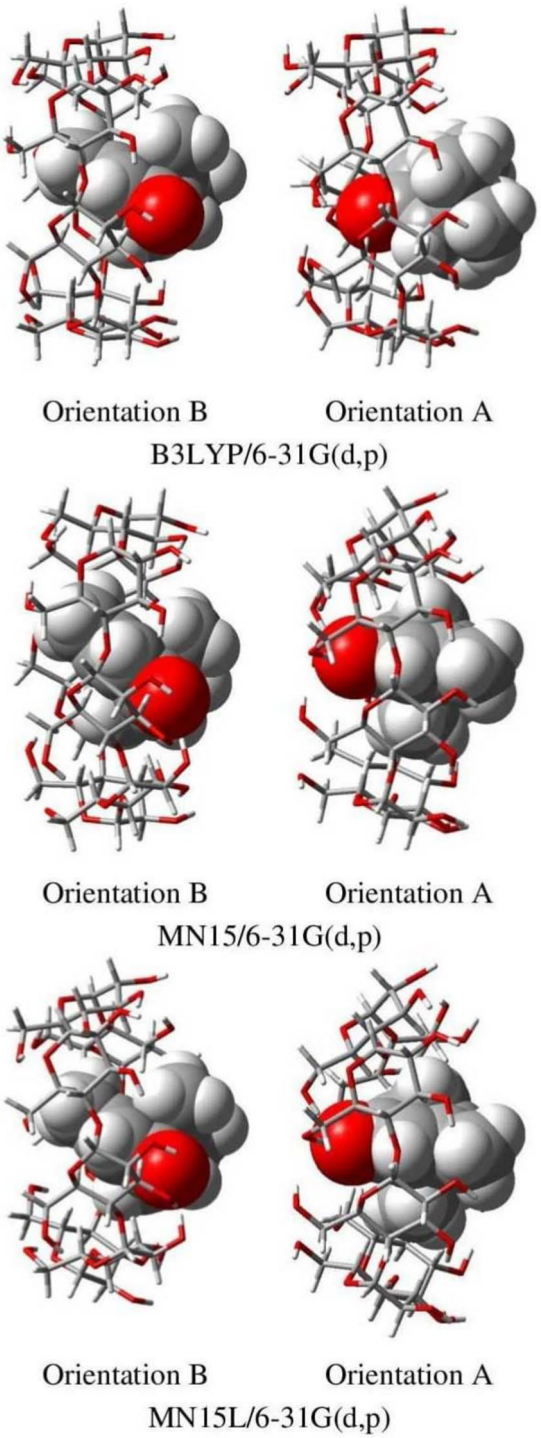

Fig. 4 The geometric representation of the optimal conformations obtained from the methods B3LYP/6–31 G(d,p), MN15/6–31 G(d,p), and MN15/6–31 G(d,p) in orientation A and B in water

cyclodextrin complex. The analysis focused on two molecular orbitals: the highest occupied molecular orbital (HOMO), which donates electrons, and the lowest unoccupied molecular orbital (LUMO), which accepts electrons. According to Koopmans' theory [34], the energies of these two orbitals, E_{HOMO} and E_{LUMO}, are directly related to the ionization potential *(I)* and the electron affinity *(A)*. Both HOMO and LUMO play critical roles as chemical indicators in this investigation. Global reactivity indices are used to calculate critical reactivity parameters, including electronic potential (μ) [34–36], hardness (η) [37], global electrophilicity index (ω) [38], maximum electronic charge transfer (ΔN_{max}) [39], and electrophilicity based charge transfer (ECT) [40]. Table 3 summarizes the HOMO, LUMO energy values, as well as reactivity parameters, for the Verb*β−cyclodextrin complex obtained using the MN15/6–31(d,p) and MN15L/6–31(d,p) methods at orientations A and B in aqueous phases. The value of the $\Delta E_{(\mathrm{HOMO\text{-}LUMO})}$ gap reflects the stability of the complex; the complex's stability improves as this value increases. According to findings in Table 3, orientation A in the aqueous phase has a larger $\Delta E_{(\mathrm{HOMO\text{-}LUMO})}$ gap value than orientation B for both methods. Thus, it indicates that the complex in orientation A is more stable than in orientation B. This finding is consistent with the recalculation of interaction and complexation energies. The chemical potential (μ) determines the direction of electron movement in an inclusion system. It is defined as electrons moving from a molecule with a higher chemical potential to another with a lower chemical potential; so, in this study, electrons move from the host to the guest. The negative value of this potential indicates that inclusion occurs spontaneously and that the complex remains stable. We confirmed the direction and stability of charge transfer using the electrophilicity index and ECT. Electrophilicity refers to the ability to attract electrons; the more electrophilic a complex, the more stable it is. Verbenone is more electrophilic than β−CD, resulting in a more electrophilic complex at orientation A compared to orientation B. The negative ECT transfers the charge from the β−CD to the verbenone. However, orientation A is more stable than orientation B. Hardness (η) confirms the complex's stability by measuring resistance to changes in electronic distribution within the molecule. A complex with higher hardness is stable, indicating that orientation A is more stable than orientation B. Figure 5 depicts the location of the HOMO and LUMO orbitals for the Verb*β−cyclodextrin complex, calculated using the

Table 3 The global reactivity indexes of β−cyclodextrin, Verbenone, and the Verb*β−CD complex in the MN15/6–31 G(d,p) and MN15L/6–31 G(d,p) methods in both orientations and in the aqueous phase

	In aqueous phase			
	Free Verb	Free β−CD	Orientation A	Orientation B
	MN15/MN15L			
$E_{\mathrm{HOMO}}(eV)$	− 7.6050/− 5.8341	− 8.0396/− 6.3007	− 8.1049/− 6.2697	− 7.8526/− 6.0046
$E_{\mathrm{LUMO}}(eV)$	− 0.4949/− 1,8032	2, 2958/0, 9461	− 1.2579/− 2.3752	− 1.1012/− 2.1194
$\Delta E_{gap}(eV)$	7.1101/4.0309	10, 3354/7.2468	6.847/3.8944	6.7514/3.8852
μ(eV)	− 4.0499/− 3.8186	− 2,8719/− 2.6773	− 4.6814/− 4.3224	− 4.4769/− 4.062
χ(eV)	4.0499/3.8186	2, 8719/2.6773	4.6814/4.3224	4.4769/4.069
η(eV)	3.5550/2.0154	5, 1677/3.6234	3.4235/1.9472	3.3757/1.9426
ω(eV)	2.3068/3.6175	0.7980/0.9891	3.2007/4.7974	2.9686/4.2468
ΔN_{max}	1.1392/1.8947	0.5557/0.7388		
ECT	− 0.5835/− 1.1559			

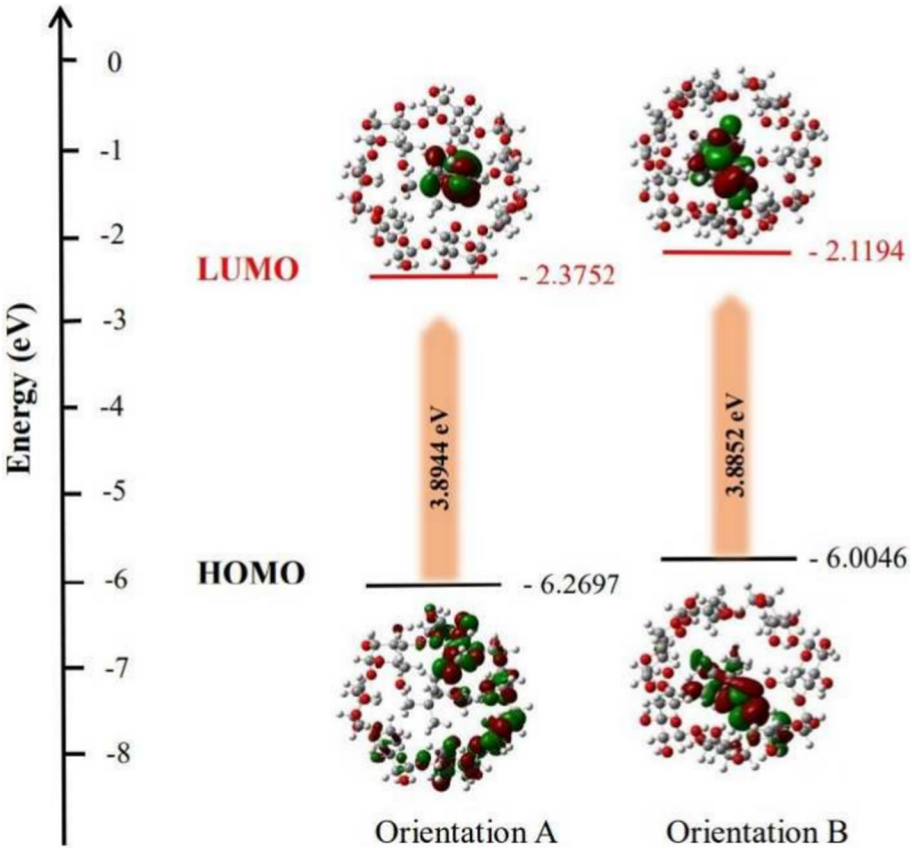

Fig. 5 Schematic diagram of HOMO and LUMO orbital obtained with MN15L/6–31 G(d,p) method at orientation A and B in aqueous phase

MN15L/6–31 G(d,p) method in orientations A and B. In orientation A, the HOMO orbitals are primarily located on $\beta-$CD, while the LUMO orbitals are entirely located on the verbenone molecule. In the B orientation, it can be noted that, in addition to all the LUMO orbitals, verbenone contains the majority of the HOMO orbitals. The results show charge transfer between $\beta-$CD and verbenone, which is more significant for orientation A compared to orientation B.

3.3 Natural Bond Orbital Analysis

Natural bond orbital (NBO) analysis was performed using Gaussian 16 and the MN15/6–31(d,p) and MN15L/6–31(d,p) methods. The NBO analysis was used to better understand the intermolecular interactions and charge transfer between occupied (donor) and unoccupied (acceptor) orbitals. The stabilization energy value, E2, determines the strength of orbital interaction. The higher the energy, the stronger the interaction [41, 42]. Table 4 displays the most significant interactions between donor and acceptor orbitals for orientations A and B in the aqueous medium, using the MN15/6–31(d,p) and MN15L/6–31(d,p) methods. According to the results, there are two different types

Table 4 The stabilization energies E2 of the most important charge transfer between the donor and acceptor orbitals calculate for the best methods MN15/6–31 G(d,p) and MN15L/6–31 G(d,p) in both orientations in water

Donor	Acceptor	E^2(kJ · mol^{-1})	
		MN15/	MN15L
Orientation A			
$\beta-$CD	Verbenone		
BD(1) C_{63}-H_{134}	BD*(1)C_{157}-H_{158}	3.26	2.13
LP(1) O_{29}	BD*(1) C_{168}-H_{171}	25.37	18.85
LP(2) O_{29}	BD*(1) C_{150}-H_{172}	2.55	2.17
LP(1) O_{62}	BD*(1) C_{153}-H_{155}	5.10	0.63
verbenone	$\beta-$CD		
LP(1) O_{167}	BD*(1) O_{33}-H_{107}	41.26	16.89
LP(2) O_{167}	BD*(1) O_{33}-H_{107}	27.21	14.84
LP(1) O_{167}	BD*(1) O_{22}-H_{97}	37.58	15.51
LP(2) O_{167}	BD*(1) O_{22}-H_{97}	25.21	13.75
Orientation B			
$\beta-$CD	Verbenone		
LP(2) O_{55}	BD*(1) C_{168}-H_{170}	4.97	–
LP(1) O_{18}	BD*(1) C_{164}-H_{165}	4.31	–
LP(1) O_{29}	BD*(1) C_{168}-H_{171}	6.65	2.97
LP(2) O_{27}	BD*(1) C_{157}-H_{159}	4.56	47
LP(2) O_{25}	BD*(1) C_{153}-H_{154}	–	3.76
LP(1) O_{73}	BD*(1) C_{161}-H_{162}	–	2.80
Verbenone	$\beta-$CD		
BD(2) C_{151}-O_{167}	BD*(1) O_{69}-H_{140}	6.31	12.75
LP(1) O_{167}	BD*(1) O_{69}-H_{140}	39.58	5.51
LP(2) O_{167}	BD*(1) $C_{69}-H_{140}$	38.33	11.95

of bonds: non-covalent hydrogen bonds between (LP) and (BD*) and van der Waals interactions localized between (BD) and (BD*). In orientation A, the two methods, MN15/6–31(d,p) and MN15L/6–31(d,p), have identical significant interactions. When the host is the donor, and the guest is the acceptor, a single van der Waals interaction is detected between the bonding orbital C63-H134 and the anti-bonding orbital C157-H158. The energy stabilization is 3.26 kJ · mol^{-1} for the MN15/6–31(d,p) method and 2.13 kJ · mol^{-1} for the MN15L/6–31(d,p) method. The isolated oxygen pairs of the glycidyl bond of $\beta-$CD are also involved. It can be noted that the highest stabilization energy E2 corresponds to the charge transition between the lone pair of O29 and the anti-bonding orbital C150-H171 with values of 25.37 kJ · mol^{-1} for the MN15/6–31(d,p) method and 18.85 kJ · mol^{-1} for the MN15L/6–31(d,p) method. When the guest is considered a donor and the host is an acceptor, four hydrogen bonds are formed mainly between the free oxygen pairs of verbenone's ketone function O167 and the anti-bonding orbitals O33-H107 and O22-H97. The charge transition from LP (O167) to BD* (O33-H107) has the highest stabilization energy value, 41.26 kJ · mol^{-1} for the MN15/6–31(d,p) method and 16.89 kJ · mol^{-1} for the MN15L/6–31(d,p) method. When the host acts as a donor in orientation B, the two methods have only two interactions in common. The first is between the non-bonding orbital of O29 and the anti-bonding orbital C168-H171, with an energy of 6.65 kJ · mol^{-1} for the MN15/6–31(d,p) method and 2.96 kJ · mol^{-1} for the MN15L/6–31(d,p)

method. The second is noted between the non-bonding orbital of O27 and the anti-bonding orbital C157-C159, with an energy of 4.56 kJ · mol^{-1} for the MN15/6–31(d,p) method and 4.47 kJ · mol^{-1} for the MN15L/6–31(d,p) method. When the guest acts as a donor, a van der Waals interaction is formed between the bonding orbital C151-O167 and the anti-bonding orbital O69-H140. In addition, two hydrogen bonds are detected between the non-bonding orbital of O167 and the anti-bonding orbital of O69-H170. The NBO results show that the verb*β−cyclodextrin complex is stable due to hydrogen bonds and van der Waals interactions. The results are in good agreement with experimental observations in [11], which underline that the enthalpy changes (ΔH) associated with the complex formation are relatively large; in contrast, the entropy changes (ΔS) are small and negative in both aqueous and (DES:water) media. These thermodynamic parameters indicate that the complex's formation is primarily enthalpy-driven, implying that van der Waals forces play an important role in its stabilization.

3.4 QTAIM Analysis

One of the most insightful studies to confirm the concrete formation of a complex is the discovery of intermolecular interactions between the two fragments that comprise this complex. The QTAIM analysis offers a comprehensive understanding of the interactions within the molecular system based on the topological parameters of the critical points of the bonds. A critical point of a bond (BCP) is the point with no electron density gradient [43]. In this study, we selected the critical points of the most significant chemical bonds discussed previously in the NBO analysis. Figure 6 highlights the critical points of the selected interactions at orientations A and B in both methods, MN15/6–31 G(d,p) and MN15L/6–31 G(d,p). These CPs appear as an orange dot in the middle of the interaction. Tables S1 and S2 (supplementary data) reveal the topological parameters (ρ, $\nabla 2\rho$, G(r), V(r), H(r), E_{int}) of the most significant intermolecular interactions for the MN15/6–31 G(d,p) and MN15L/6–31 G(d,p) methods at orientations A and B. The intermolecular interaction's nature is determined by the Laplacian ($\nabla 2\rho$) and the electron density (ρ). A low electronic density and a Laplacian$\nabla 2\rho > 0$ are characteristics of a weak non-covalent link, whereas a high ρ and a Laplacian $\nabla 2\rho < 0$ denote a covalent bond [42]. By employing this reference alongside our findings, we note that each critical point is linked to non-covalent intermolecular interactions. The study presented in [44, 46] indicates that the type of non-covalent bond can be identified by examining the total electrical energy density H(r): a medium hydrogen bond with partial covalence has a positive Laplacian and $H(r) < 0$; in contrast, a weak hydrogen bond or van der Waals interaction has a positive Laplacian and $H(r) > 0$. It can be described using Eq. 4 [47]:

$$H(r) = G(r) + V(r), \tag{4}$$

where G(r) is the kinetic energy density, and V(r) is the potential (negative value).

When H(r) is negative, it indicates that $G(r) < V(r)$, signifying a high concentration of electronic charge in the intermolecular region, which facilitates the formation of a covalent bond or a robust hydrogen bond. Simultaneously, when H(r) is positive, it indicates that $G(r) > V(r)$, resulting in a greater concentration of electronic charge near the nucleus; consequently, this facilitates the formation of weak hydrogen bonds or van der Waals interactions. According to Tables S1 and S2, the interactions 97 H-167O and 172 H-29O detected in orientation A correspond to medium hydrogen bonds. The values obtained are −0.00036 for the MN15/6–31 G(d,p) method and

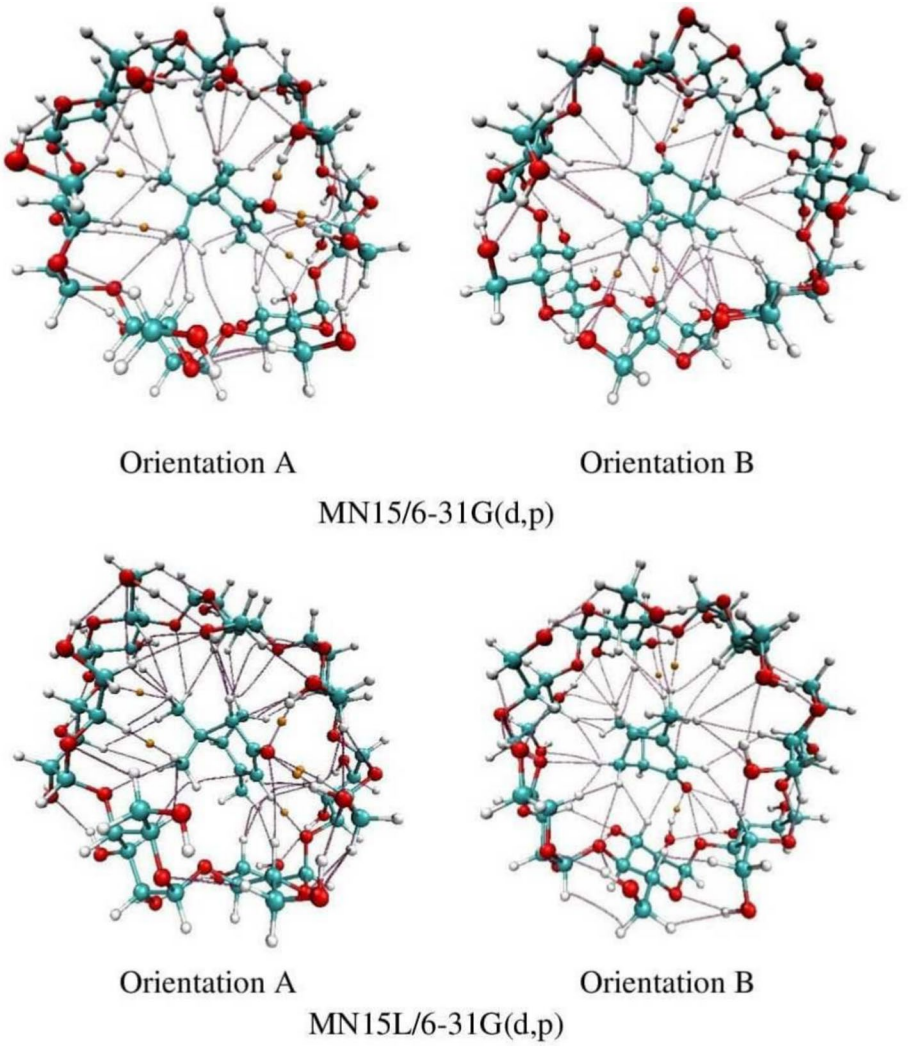

Fig. 6 QTAIM molecular topography showing the bond critical points and bond paths of the Verb*β–cyclodextrin complex at A and B orientations given by MN15/6–31 G(d,p) and MN15L/6–31 G(d,p) methods in water phase (Color figure online)

-0.00069 for the MN15L/6–31 G(d,p) method for the 97 H-167O interaction, −0.00077 for the MN15/6–31 G(d,p) method, and −0.00058 for the MN15L/6–31 G(d,p) method for the 172 H-29O interaction. Additionally, the two hydrogen bonds 170 H-167O at orientation A and 140 H-167 H at orientation B exhibit weak interactions ($H(r) > 0$) for the MN15/6–31 G(d,p) method and medium interactions ($H(r) < 0$) for the MN15L/6–31 G(d,p) method. The rest of the interactions are considered weak hydrogen bonds with a van der Waals interaction between 134 H and 158 H having a value of 0.0011 calculated by the MN15/6–31 G(d,p) method and a value of 0.0012 calculated

by the MN15L/6–31 G(d,p) method. Medium-intensity hydrogen bonds have the lowest interaction energies.

3.5 NCI-RDG Analysis

A non-covalent interaction analysis method (NCI) based on reduced density gradient studies (RDG) was developed to better understand the nature of the host-guest interaction. This method allows the graphic visualization of regions where non-covalent interactions occur in real space. In the study [48], researchers developed RDG to quantify non-covalent interactions. This approach is based on electron density and its first derivative. It can be described using Eq. 5.

$$RDG(r) = (1 \mid \bigtriangledown \rho(r))/(2(3\pi^2)^{1/3}\rho(r)^{4/3}. \tag{5}$$

Figure 7 shows a 2D RDG plot as a function of ρ multiplied by λ_2, which is the sign of the second eigenvalue of the Laplacian density [49]. The value of the sign λ_2 determines the nature of the interaction. For example, $\lambda_2 < 0$ indicates attractive interactions like hydrogen bonds (region colored in blue), while $\lambda_2 = 0$ indicates van der Waals interaction (region colored in green); $\lambda_2 > 0$ represents a repulsive interaction (region colored in red).

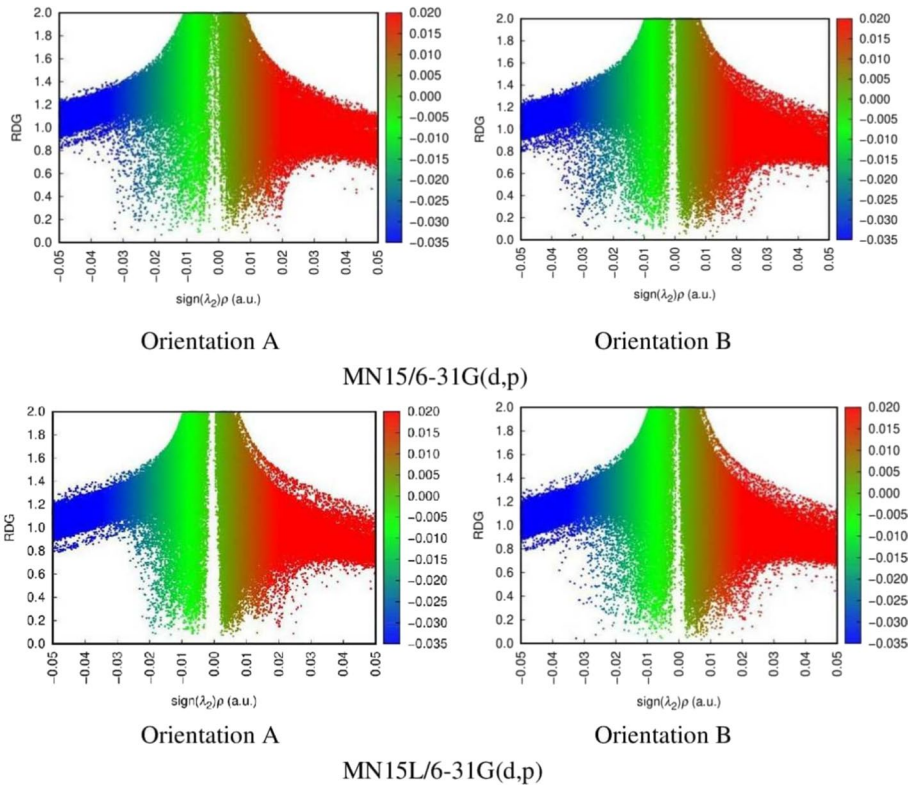

Fig. 7 The 2D RDG plot for MN15/6–31(d,p) and MN15L/6–31(d,p) methods at orientation A and B (Color figure online)

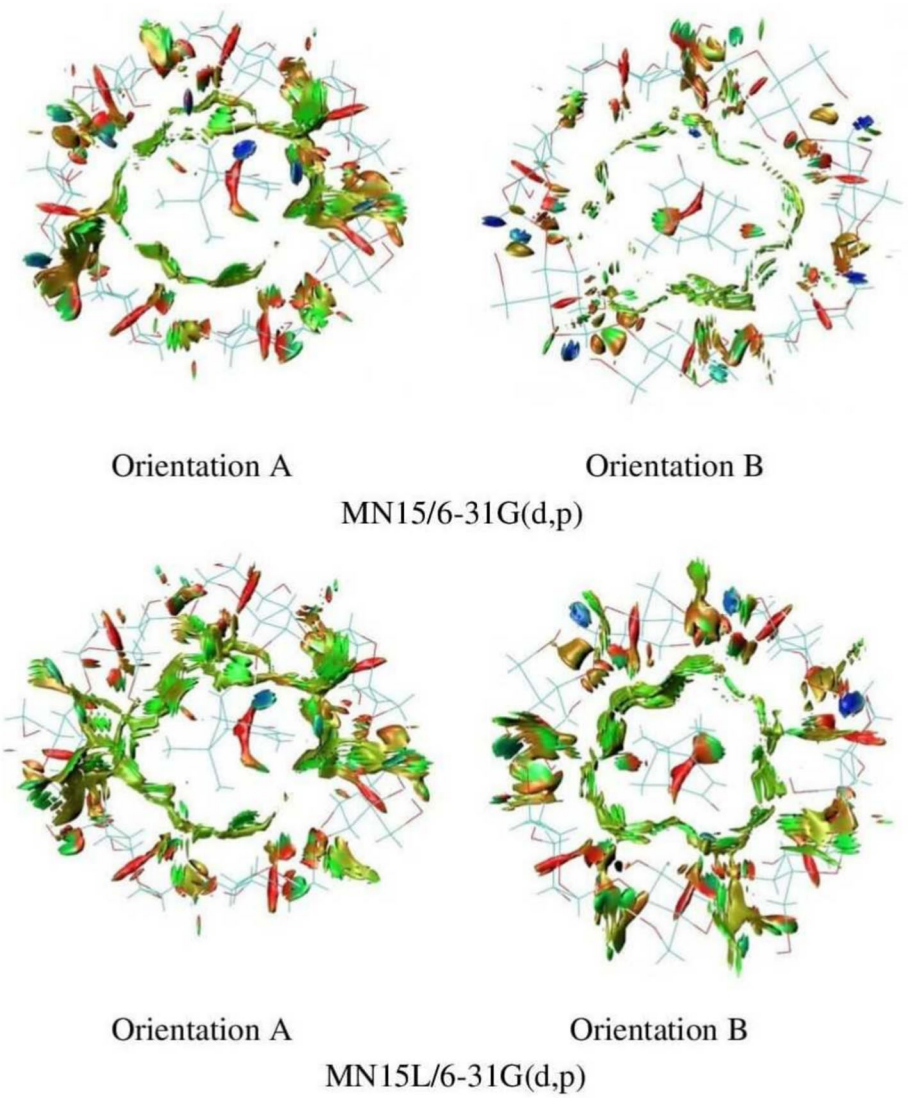

Fig. 8 The 3D NCI isosurfaces for the MN15/6–31(d,p) and MN15L/6–31(d,p) methods in orientations A and B in the aqueous phase (Color figure online)

Figure 8 illustrates 3D NCI isosurface plots for the MN15 and MN15L methods at orientations A and B. The green spot, representing van der Waals interactions, takes up a significant portion of the space between the $\beta-$CD and verbenone, as opposed to the blue and red spots. These findings suggest that non-covalent interactions, particularly van der Waals interactions, are critical to the complex's formation and stability.

3.6 IGM Analysis

Unlike NCI analysis, which combines all non-covalent intra- and intermolecular interactions, independent gradient model (IGM) analysis allows these interactions to be quantified individually. It is expressed as Eq. 6 [50].

$$\delta g^{\mathrm{IGM}} = \delta g^{\mathrm{intra}} + \delta g^{\mathrm{inter}}, \tag{6}$$

where $\delta g^{\mathrm{intra}}$ and $\delta g^{\mathrm{inter}}$, respectively, indicate the intramolecular and intermolecular interactions between the two fragments.

Figure 9 depicts scatterplots of $\delta g^{\mathrm{intra}}$ and $\delta g^{\mathrm{inter}}$ as a function of sing $(\lambda_2)\rho$ for the Verb*β−cyclodextrin complex in the MN15/6–31(d,p) and MN15L/6–31(d,p) methods at orientations A and B in the aqueous phase. The black dots represent intramolecular interactions, while the red dots represent intermolecular interactions. The MN15/6–31(d,p) and MN15L/6–31(d,p) methods have the most intense black point peak in the negative region, with a song $(\lambda_2)\rho \approx -0.22$ (a.u) for both orientations. The MN15/6–31(d,p) method yielded peaks with a height of 0.487 for orientation A and 0.491 for orientation B. Using the MN15L/6–31(d,p) method, the height was 0.467 for orientation A and 0.482 for

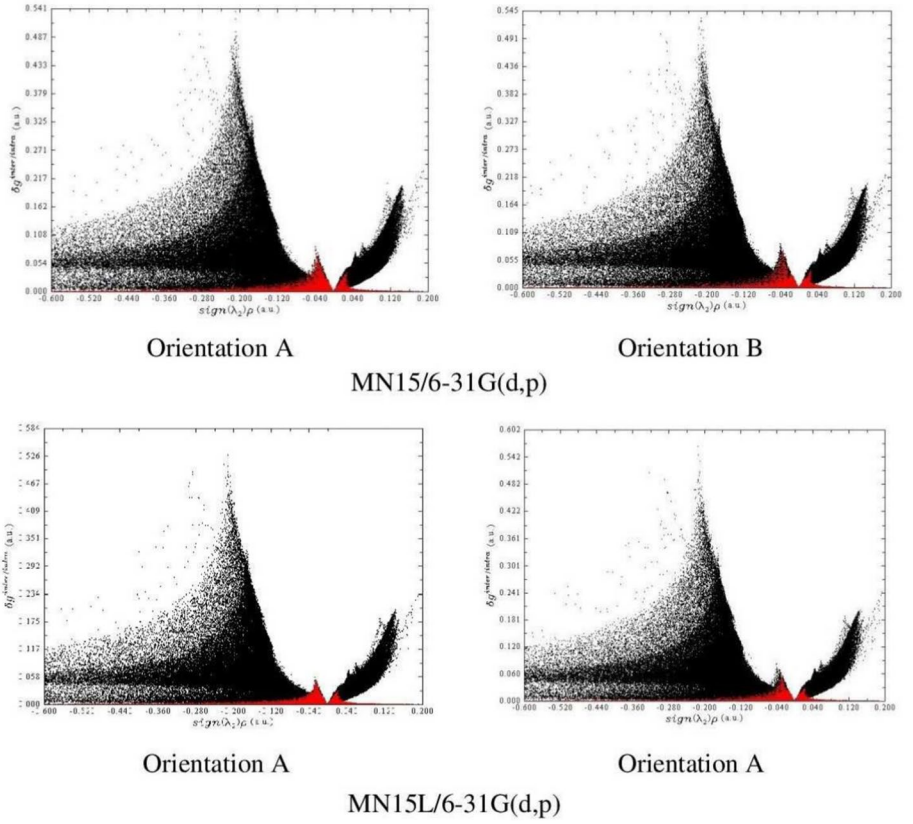

Fig. 9 The scatter plots of the intra- and interfragment interactions within the complex for the MN15/6–31(d,p) and MN15L/6–31(d,p) methods in orientations A and B in the aqueous phase (Color figure online)

orientation B. The highest peak of red dots for both methods also appeared in the negative region with singing $(\lambda_2)\rho \approx -0.04$ (a.u.) for both orientations. Using the MN15/6–31(d,p) method, the red peaks had a height of 0.055 for orientation A and 0.057 for orientation B, while the height was 0.058 for orientation A and 0.060 for orientation B, with the MN15L/6–31(d,p) method. For this analysis, the MN15/6–31(d,p) and MN15L/6-31(d,p) methods yielded nearly identical results, indicating that the two methods produce the same intensity of intra- and intermolecular interactions. The colored IGM scatter map in Fig. 10 and its visualization in Fig. 11 reveal the interactions between the fragments. The blue region between $(\lambda_2)\rho \approx -0.05$; 0.02 (a.u) represents hydrogen interaction; the green one between $(\lambda_2)\rho \approx -0.02$; 0.02 (a.u) represents van der Waals interactions; and finally, the red one corresponds to the repulsive interactions that appeared between $(\lambda_2)\rho \approx -0.02$; 0.05 (a.u), and this for orientations A and B in both methods. It can, therefore, be noted that van der Waals interactions are higher than hydrogen and repulsive interactions, meaning that the van der Waals interaction contributes most to the stability of the Verb*β–cyclodextrin complex. These findings are consistent with the results of the NCI analyses.

The complementary $\delta g^{\text{inter/At}}$ analysis, which assigns the atomic contributions of host and guest molecules, was carried out to better understand which atoms participate most in intermolecular interactions. Figure 12 shows the IGM analysis with a δg^{inter}

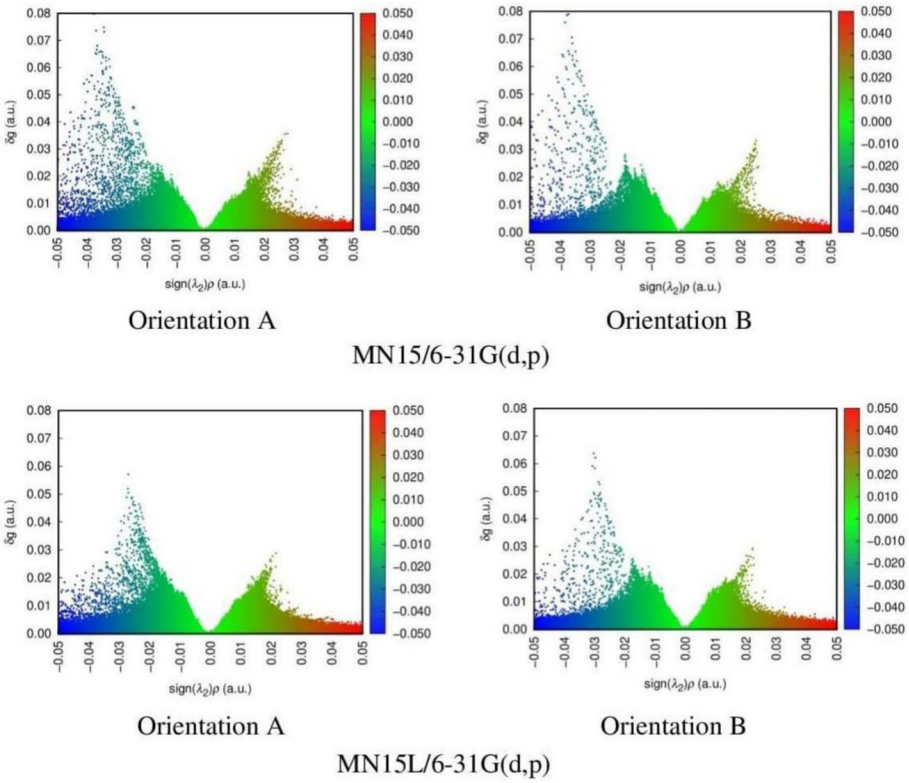

Fig. 10 The colored IGM scatterplots of the interfragment interactions of the complex for the MN15/6–31(d,p) and MN15L/6–31(d,p) methods in orientations A and B in the aqueous phase (Color figure online)

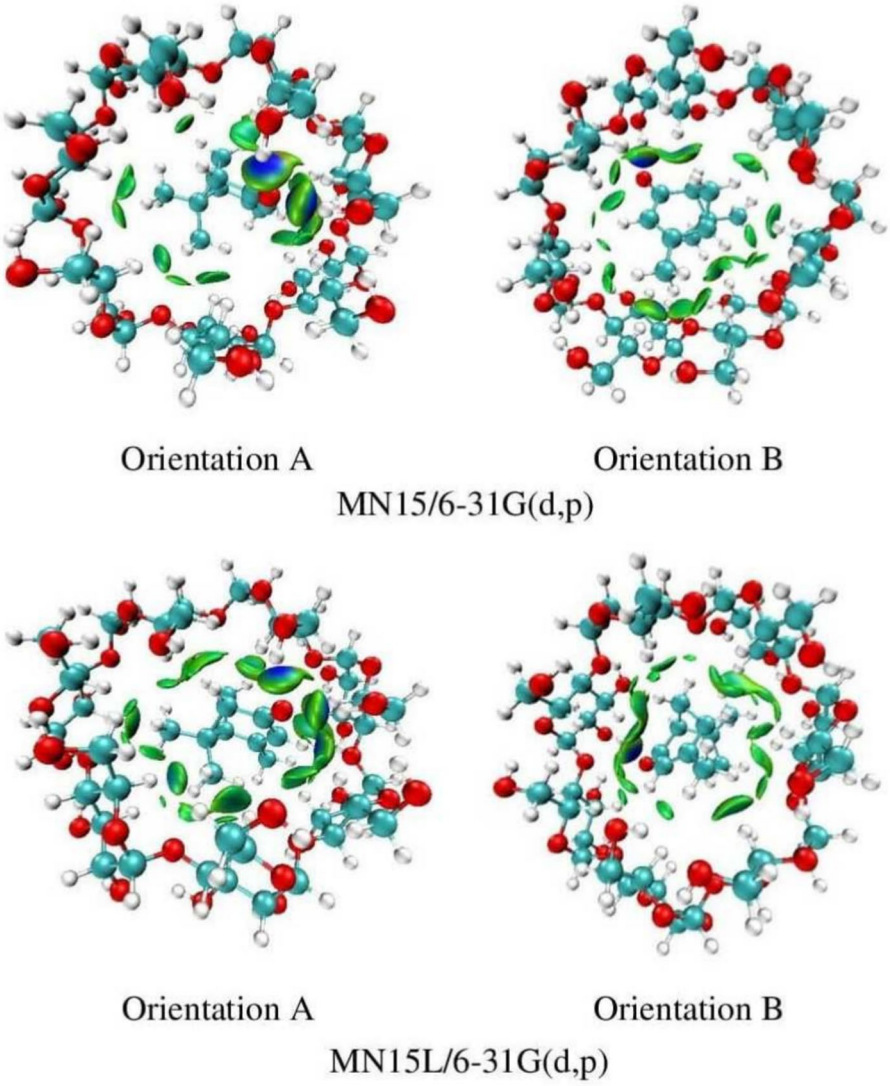

Fig. 11 The 3D IGM isosurface of the complex for the MN15/6–31(d,p) and MN15L/6–31(d,p) methods in orientations A and B in the aqueous phase (Color figure online)

isosurface of 0.004 a.u. Host and guest are colored according to $\Delta G^{\text{inter/At}}$ score for the MN15/6–31(d,p) and MN15L/6–31(d,p) methods at orientations A and B, respectively. Verbenone is more involved in intermolecular interactions than β−CD, as evidenced by the color difference between the guest and host molecules. The darker-colored host atoms contribute most to these interactions. Verbenone's O167 strongly interacts with hydroxide groups of β−CD, O22-H107, O33-H97 for orientation A, and O69-H140 for orientation B; van der Waals interactions between the two fragments (CH...CH and

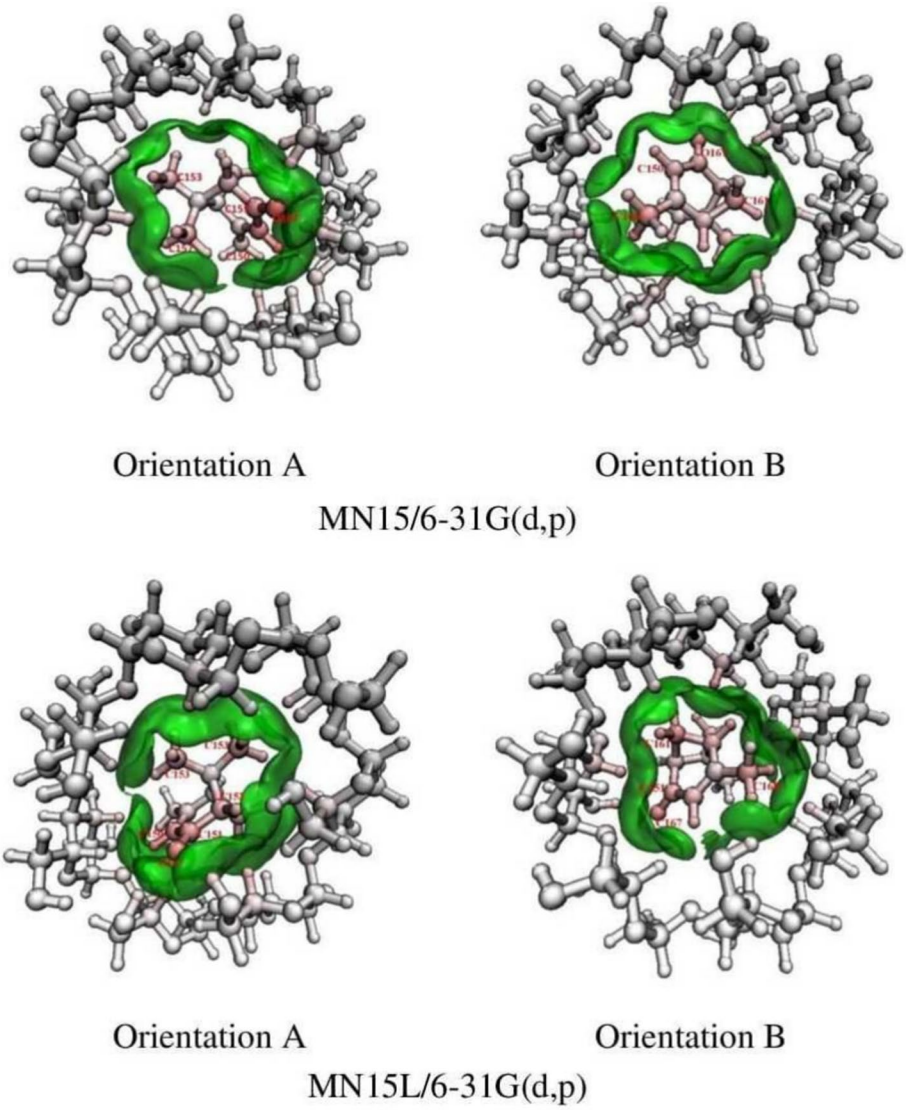

Fig. 12 Host and guest colored according to the $\Delta g^{inter/At}$ score for methods MN15/6–31(d,p) and MN15L/6–31(d,p) at orientations A and B in the aqueous phase (Color figure online)

CH...O) can also be observed. The results of this analysis confirm the presence of all non-covalent intermolecular interactions previously identified in the NBO analysis and supported by NCI analyses.

3.7 ^{1}H NMR Analysis

The NMR technique was used to confirm verbenone encapsulation in the β−cyclodextrin cavity. This technique allows us to confirm the encapsulation of a guest molecule by

Table 5 Chemical shift values of Verbenone protons before and after complexation

Calculated				Experimental
Protons	$\delta_{\text{free verb}}$	δ_{verb}in orientation A	δ_{verb}in orientation B	$\delta_{\text{free verb}}$
162-H	2.34	3.01	3.09	2.08 – 2.10(*m*)
163-H	3.10	3.52	3.83	2.80 – 2.91(*m*)
165-H	2.65	2.92	3.54	2.42
166-H	2.90	3.37	3.28	2.62 – 2.70(*m*)
169-H	2.26	2.36	3.04	1.92
170-H	2.31	3.38	3.12	2
171-H	2.40	2.69	2.93	2.1
172-H	6.14	7.94	6.79	5.71

$u(\delta_{free\ verb}\ calc) = +/-0.4$

observing the change in its chemical shift. If the guest molecule's environment changes, so does its chemical shift, confirming the guest's encapsulation within the host cavity. The chemical shifts δ of selected hydrogens obtained on a large scale using TMS as a reference implemented in [51, 52] were evaluated with the independent atomic orbital method (GIAO). The B3LYP/6–311 G (+2d, p) methodology was applied by single-point calculation on geometry optimized by the MN15L/6–31(d, p) method once it was suitable for the theoretical NMR spectra of organic molecules [53, 54]. These calculations were performed without a solvent. Table 5 and Fig. 13 display the chemical shifts of verbenone isolated in addition when it is complexed in orientations A and B. Analysis of Table 5 reveals that the signs of all the protons selected after complexation are shifted toward the strong magnetic field, with protons H172 and H170 showing the largest difference between the free and complex states. It can also be observed that for all protons, the chemical shift values between orientations A and B are very close, except for the protons H169 and H172, where the difference is 0.68 and 1.15, respectively. The

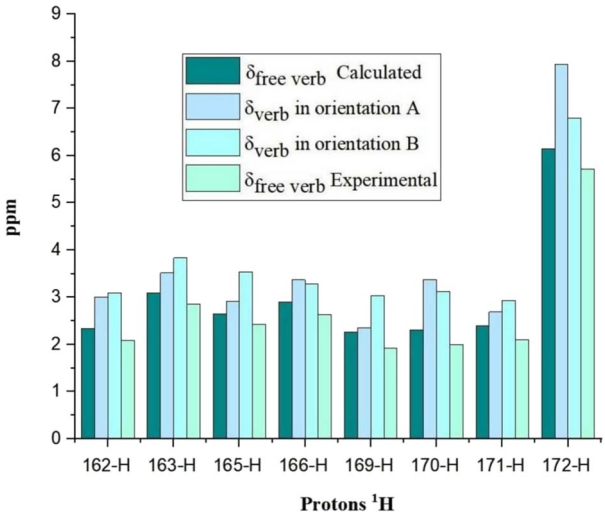

Fig. 13 Experimental [8] and calculated ^{1}H chemical shifts of verbenone in the free and encapsulated state (Color figure online)

theoretical values of the free guest molecule are in good agreement with the experimental values [8], with a slight difference due to the use of CHCl3 as a solvent in the experimental studies (Fig. 13). Thus, ^{1}H NMR results confirm that β-cyclodextrin envelops the entire guest and that the complexation is well achieved.

4 Conclusion

A computational study was carried out on the Verb*β–cyclodextrin inclusion complex, using computational methods and quantum chemical analyses to better understand the different changes undergone by verbenone and β-cyclodextrin during encapsulation. Following the complexation simulation, a PM3 semi-empirical method was employed to conduct a conformational search to identify the optimal conformations. The most stable conformations were studied energetically and structurally using the density functional theory DFT with the B3LYP, MN15, and MN15L methods, as well as a 6–31 G(d,p) basis set to correct for dispersion. The results of this study show that the complex in orientation A is more stable than that in orientation B in the gas and aqueous phases. The interaction energy, complexation energy, ΔE_{gap}, and different reactivity parameters support our findings.

Furthermore, the results of the NBO, QTAIM, NCI, and IGM analyses confirm the presence of intermolecular interactions between the host and the guest, ensuring complex formation and stability. The MN15L method appears to be the best in terms of energy, but the MN15 method presents the best results in terms of stability (ΔE_{gap}) and interaction intensity (NBO). Ultimately, ^{1}H NMR analysis demonstrated a strong correlation with experimental results. These findings encourage us to conduct additional research using other semi-empirical methods such as PM6, PM7, and other DFT methods to obtain more precise results.

Supplementary Information The online version contains supplementary material available at https://doi.org/10.1007/s10953-025-01436-5.

Acknowledgements This work was partially supported by Algerian Research Ministry, MERS.

Author Contributions Souha Fatma Zohra Soukehal was responsible for the molecule selection, semi-empirical calculation, QTAIM, NCI-RDG, and IGM studies, as well as data collection and analysis. Tahar Abbaz and Didier Villemin performed the final optimization using DFT, NBO, and NMR analysis calculations via cluster assignment. Souha Fatma Zohra Soukehal wrote the manuscript, and Bouchouk Djamel and Tahar Abbaz edited it. Souha Fatma Zohra Soukehal, Bouchouk Djamel, and Tahar Abbaz read and approved the final manuscript.

Funding The authors did not receive support from any organization for the submitted work.

Declarations

Conflict of interest The authors declare no competing interests.

References

1. Del Valle, E.M.: Cyclodextrins and their uses: a review. Proc. Biochem. **39**, 1033–1046 (2004)
2. Roy, N., Ghosh, B., Roy, D., Bhaumik, B., Roy, M.N.: Exploring the inclusion complex of a drug (umbelliferone) with α–cyclodextrin optimized by molecular docking and increasing bioavailability with minimizing the doses in human body. ACS Omega **5**, 30243–30251 (2020)

3. Halahlah, A., Kavetsou, E., Pitterou, I., Grigorakis, S., Loupassaki, S., Tziveleka, L.A., Detsi, A.: Synthesis and characterization of inclusion complexes of rosemary essential oil with Various $\beta-$cyclodextrins and evaluation of their antibacterial activity against *Staphylococcus aureus*. J. Drug. Deliv Sci. Technol. **65**, 102660 (2021)
4. Kavetsou, E., Pitterou, I., Katopodi, A., Petridou, G., Adjali, A., Grigorakis, S., Detsi, A.: Preparation, characterization, and acetylcholinesterase inhibitory ability of the inclusion complex of $\beta-$cyclodextrin-cedar (*Juniperus Phoenicea*) essential oil. In Micro **1**, 250–266 (2021)
5. Kotronia, M., Kavetsou, E., Loupassaki, S., Kikionis, S., Vouyiouka, S., Detsi, A.: Encapsulation of oregano (*Origanum Onites* L.) essential oil in $\beta-$cyclodextrin ($\beta-cd$: synthesis and characterization of the inclusion complexes. J. Bioeng. **4**, 74 (2017)
6. Saokham, P., Muankaew, C., Jansook, P., Loftsson, T.: Solubility of cyclodextrins and drug/cyclodextrin complexes. Molecules **23**, 1161 (2018)
7. Nora, M., Ismahan, L., Abdelkrim, G., Mouna, C., Leila, N., Fatiha, M., Brahim, H.: Interactions in inclusion complex of $\beta-$cyclodextrin/l-metheonine: Dft computational studies. J. Incl. Phenom. Macrocycl. Chem. **96**, 43–54 (2020)
8. Yoosuf-Aly, Z., Faraldos, J.A., Miller, D.J., Allemann, R.K.: Chemoenzymatic synthesis of the alarm pheromone (+)-verbenone from geranyl diphosphate. Chem. Commun. **48**, 7040–7042 (2012)
9. Petrovic, J., Kovalenko, V., Svirid, A., Stojkovic, D., Ivanov, M., Kostic, M.: Individual stereoisomers of verbenol and verbenone express bioactive features. J. Mol. Struct. **1251**, 131999 (2022)
10. Raffo, A., Baiamonte, I., De Benedetti, L., Lupotto, E., Marchioni, I., Nardo, N., Cervelli, C.: Exploring volatile aroma and non-volatile bioactive compounds diversity in wild populations of rosemary (Salvia Rosmarinus Schleid). Food Chem. **404**, 134532 (2023)
11. Nakhle, L., Kfoury, M., Ruellan, S., Greige-Gerges, H., Landy, D.: Insights on cyclodextrin inclusion complexes in deep eutectic solvents: water mixtures. J. Mol. Struct. **1293**, 136260 (2023)
12. Wu, Y.Y., Zhao, F.Q., Ju, X.H.: A comparison of the accuracy of semi-empirical PM3, PDDG and PM6 methods in predicting heats of formation for organic compounds. J. Mex. Chem. Soc. **58**, 223–229 (2014)
13. Rezac, J., Hobza, P.: Advanced corrections of hydrogen bonding and dispersion for semi empirical quantum mechanical methods. J. Chem. Theory Comput. **8**, 141–151 (2012)
14. Stewart, J.J.: Optimization of parameters for semiempirical methods VI: more modifications to the NDDO approximations and re-optimization of parameters. J. Mol. Model. **19**, 1–32 (2013)
15. Tirado-Rives, J., Jorgensen, W.L.: Performance of B3LYP density functional methods for a large set of organic molecules. J. Chem. Theory Comput. **4**, 297–306 (2008)
16. Haoyu, S.Y., He, X., Li, S.L., Truhlar, D.G.: MN15: a Kohn-Sham global-hybrid exchange-correlation density functional with broad accuracy for multi-reference and single-reference systems and noncovalent interactions. Chem. Sci. **7**, 5032–5051 (2016)
17. Yu, H.S., He, X., Truhlar, D.G.: MN15-L: a new local exchange-correlation functional for Kohn-Sham density functional theory with broad accuracy for atoms, molecules, and solids. J. Chem. Theory Comput. **12**, 1280–1293 (2016)
18. Kim, S., Chen, J., Cheng, T., Gindulyte, A., He, J., He, S., Bolton, E.E.: Pubchem in 2021: new data content and improved web interfaces. Nucleic Acids Res. **49**, 1388–1395 (2021)
19. Hypercube, I.: HyperChem(TM) Professional 8.0. Gainesville (2007)
20. Frisch, M.E., Trucks, G.W., Schlegel, H.B., Scuseria, G.E., Robb, M.A., Cheeseman, J.R., Fox, D.J.: Gaussian 16, Revision C.01. Gaussian Inc, Wallingford (2016)
21. Dennington, R., Keith, T.A., Millam, J.M.: GaussView, Version 6. Semichem Inc, Shawnee Mission (2019)
22. Lu, T., Chen, F.: Multiwfn: a multifunctional wavefunction analyzer. J. Comput. Chem. **33**, 580–592 (2012)
23. Spivak, M., Stone, J.E., Ribeiro, J., Saam, J., Freddolino, P.L., Bernardi, R.C., Tajkhorshid, E.: VMD as a platform for interactive small molecule preparation and visualization in quantum and classical simulations. J. Chem. Inf. Model. **63**, 4664–4678 (2023)
24. Williams, T., Kelley, C.: Gnuplot 4.5: an interactive plotting program 2011 (2017)
25. Safia, H., Ismahan, L., Abdelkrim, G., Mouna, C., Leila, N., Fatiha, M.: Density functional theories study of the interactions between host $\beta-$cyclodextrin and guest 8-anilinonaphthalene-1-sulfonate: molecular structure, HOMO, LUMO, NBO, QTAIM and NMR analyses. J. Mol. Liq. **280**, 218–229 (2019)
26. Belhouchet, H.R., Abbaz, T., Bendjedou, A., Gouasmia, A., Villemin, D.: A computational study of the inclusion of $\beta-$cyclodextrin and nicotinic acid: Dft, DFT-D, NPA, NBO, QTAIM, and NCI-RDG studies. J. Mol. Model. **28**, 348 (2022)

27. Rahim, M., Madi, F., Nouar, L., Bouhadiba, A., Haiahem, S., Khatmi, D.E., Belhocine, Y.: Driving forces and electronic structure in β−cyclodextrin/3, 3'- diaminodiphenylsulphone complex. J. Mol. Liq. **199**, 501–510 (2014)
28. Rahim, M., Madi, F., Nouar, L., Haiahem, S., Fateh, D., Khatmi, D.: β−cyclodextrin interaction with Edaravone: molecular modeling study. Adv. Quantum Chem. **68**, 269–278 (2014)
29. Abe, S., Hirota, T., Kiba, T., Miyakawa, N., Watari, F., Murayama, A., Sato, S.I.: Photophysical Properties of self-assembled cyanine-dye dimmer formation assisted by cyclodextrin inclusion complexation. Mol. Cryst. Liq. **579**, 22–29 (2013)
30. Al-Ahmary, K.M., Habeeb, M.M., Aljahdali, S.H.: Synthesis, spectroscopic studies and DFT/TD-DFT/PCM calculations of molecular structure, spectroscopic characterization and NBO of charge transfer complex between 5-amino-1, 3-dimethylpyrazole (5-ADMP) with chloranilic acid (CLA) in different solvents. J. Mol. Liq. **277**, 453–470 (2019)
31. Sundari, C.D.D., Martoprawiro, M.A., Ivansyah, A.L.: A DFT and TDDFT study of PCM effect on N3 dye absorption in ethanol solution. J. Phys: Conf. Ser. **812**, 012068 (2017)
32. Leila, N., Sakina, H., Bouhadiba, A., Madi, F.: Theoretical study of inclusion complexation of 3-amino-5-nitrobenzisothiazole with β−cyclodextrin. J. Mol. Liq. **160**, 8–13 (2011)
33. Bautista-Renedo, J.M., Hernandez-Esparza, R., Cuevas-Yanez, E., Reyes-Perez, H., Vargas, R., Garza, J., Gonzalez-Rivas, N.: Deformations of cyclodextrins and their influence to form inclusion compounds. Int. J. Quantum Chem. **122**, 26859 (2022)
34. Terayama, K., Osaki, Y., Fujita, T., Tamura, R., Naito, M., Tsuda, K., Sumita, M.: Koopmans'theorem-compliant long-range corrected (KTLC) density functional mediated by black-box optimization and data-driven prediction for organic molecules. J. Chem. Theory Comput. **19**, 6770–6781 (2023)
35. Zhan, C.G., Nichols, J.A., Dixon, D.A.: Ionization Potential, electron affinity, electronegativity, hardness, and electron excitation energy: molecular properties from density functional theory orbital energies. J. Phys. Chem. A **107**, 4184–4195 (2003)
36. Verma, P., Srivastava, A., Srivastava, K., Tandon, P., Shimpi, M.R.: Molecular structure, spectral investigations, hydrogen bonding interactions and reactivity property relationship of caffeine-citric acid cocrystal by experimental and DFT approach. Front. Chem. **9**, 708538 (2021)
37. Shafiq, I., Khalid, M., Braga, A.A., Tariq, Z., Alhokbany, N., Chen, K.: Exploration the effect of selenophene moiety and benzothiophene based acceptors on optical nonlinearity of d $-\pi-$ abased heterocyclic organic compounds in chloroform solvent: a DFT approach. J. Mol. Liq. **393**, 123569 (2024)
38. Rios-Gutierrez, M., Saz Sousa, A., Domingo, L.R.: Electrophilicity and nucleophilicity scales at different DFT computational levels. J. Phys. Org. Chem. **36**, 4503 (2023)
39. Chen, H., Ji, H.: Alkaline hydrolysis of cinnamaldehyde to benzaldehyde in the presence of β−cyclodextrin. AIChE J. **56**, 466–476 (2010)
40. Padmanabhan, J., Parthasarathi, R., Subramanian, V., Chattaraj, P.K.: Electrophilicity-based charge transfer descriptor. J. Phys. Chem. A **111**, 1358–1361 (2007)
41. Zaboli, M., Raissi, H.: The analysis of electronic structures, adsorption properties, NBO, QTAIM and NMR parameters of the adsorbed hydrogen sulfide on various sites of the outer surface of aluminum phosphide nanotube: a DFT study. Struct. Chem. **26**, 1059–1075 (2025)
42. Kumar, A.R., Selvaraj, S., Mol, G.S., Selvaraj, M., Ilavarasan, L., Pandey, S.K., Ravi, A.: Synthesis, Solvent-solute interactions (polar and non-polar), spectroscopic insights, topological aspects, Fukui functions, molecular docking, ADME, and donor-acceptor investigations of 2-(trifluoromethyl) benzimidazole: a promising candidate for antitumor pharmacotherapy. J. Mol. Liq. **393**, 123661 (2024)
43. Nkungli, N.K., Ghogomu, J.N.: Theoretical analysis of the binding of iron (III) protoporphyrinix to 4-methoxyacetophenone thiosemicarbazone via DFT-D3, MEP, QTAIM, NCI, ELF, and lol studies. J. Mol. Model. **23**, 1–20 (2017)
44. Lu, T., Chen, F.: Bond Order analysis based on the Laplacian of electron density in fuzzy overlap space. J. Phys. Chem. A **117**, 3100–3108 (2013)
45. Nguyen, T.H., Nguyen, T.H., Le, T.T.T., Vu Dang, H., Nguyen, H.M.T.: Inter actions between paracetamol and formaldehyde: theoretical investigation and topological analysis. ACS Omega **8**, 11725–11735 (2023)
46. Rozas, I., Alkorta, I., Elguero, J.: Behavior of ylides containing N, O, and C atoms as hydrogen bond acceptors. J. Am. Chem. Soc. **122**, 11154–11161 (2000)
47. Hammud, H.H., Yar, M., Bayach, I., Ayub, K.: Covalent triazine framework c6n6 as an electrochemical sensor for hydrogen-containing industrial pollutants: a DFT study. Nanomaterials **13**, 1121 (2023)
48. Johnson, E.R., Keinan, S., Mori-Sanchez, P., Contreras-Garcia, J., Cohen, A.J., Yang, W.: Revealing noncovalent interactions. J. Am. Chem. Soc. **132**, 6498–6506 (2010)
49. Rayene, K., Imane, D., Abdelaziz, B., Leila, N., Fatiha, M., Abdelkrim, G., Rabah, O.: Molecular modeling study of structures, Hirschfield surface, NBO, AIM, RDG, IGM and 1H NMR of thymoquinone/

hydroxypropyl−β−cyclodextrin inclusion complex from QM calculations. J. Mol. Struct. **1249**, 131565 (2022)
50. Lefebvre, C., Rubez, G., Khartabil, H., Boisson, J.C., Contreras-Garcia, J., Henon, E.: Accurately extracting the signature of intermolecular interactions present in the NCI plot of the reduced density gradient versus electron density. J. Phys. Chem. Chem. Phys. **19**, 17928–17936 (2017)
51. Iuliucci, R.J., Hartman, J.D., Beran, G.J.: Do models beyond hybrid density functionals increase the agreement with experiment for predicted NMR chemical shifts or electric field gradient tensors in organic solids. J. Phys. Chem. A **127**, 2846–2858 (2023)
52. Pulay, P., Hinton, J.F.: Shielding theory: Giao method. eMagRes (2007)
53. De Almeida, M.V., De Assis, J.V., Couri, M.R.C., Anconi, C.P., Guerreiro, M.C., Dos Santos, H.F., De Almeida, W.B.: Experimental and theoretical investigation of epoxide quebrachitol derivatives through spectroscopic analysis. Org. Lett. **12**, 5458–5461 (2010)
54. De Almeida, M.V., Couri, M.R.C., De Assis, J.V., Anconi, C.P., Dos Santos, H.F., De Almeida, W.B.: 1H NMR analysis of O-methyl-inositol isomers: a joint experimental and theoretical study. Magn. Reson. Chem. **50**, 608–614 (2012)

Authors and Affiliations

Souha Fatma Zohra Soukehal[1] · Djamel Bouchouk[1] · Tahar Abbaz[1] · Didier Villemin[2]

✉ Souha Fatma Zohra Soukehal
f.soukehal@univ-soukahras.dz

Djamel Bouchouk
d_bouchouk@univ-soukahras.dz

Tahar Abbaz
tahar.abbaz@univ-soukahras.dz

[1] Laboratory of Organic Chemistry and Interdisciplinary, Mohamed Cherif Messaadia University, Souk Ahras 41000, Algeria

[2] Laboratory of Molecular and Thio-Organic Chemistry of Caen, Organization, Caen 14050, France